# Inelastic electron collisions of the isotopically symmetric helium dimer ion $^4He_2^+$ in a storage ring

H. Buhr,[1,2,*] H. B. Pedersen,[1,†] S. Altevogt,[1] V. M. Andrianarijaona,[1,‡] H. Kreckel,[1,§] L. Lammich,[1,†] S. Novotny,[1] D. Strasser,[2,‖] J. Hoffmann,[1] M. Lange,[1] M. Lestinsky,[1,§] M. B. Mendes,[1] M. Motsch,[1,¶] O. Novotný,[1] D. Schwalm,[1,2] X. Urbain,[3] D. Zajfman,[1,2] and A. Wolf[1]

[1]*Max-Planck-Institut für Kernphysik, Saupfercheckweg 1, D-69117 Heidelberg, Germany*

[2]*Department of Particle Physics, Weizmann Institute of Science, Rehovot, 76100, Israel*

[3]*Laboratoire de Physique Atomique et Moléculaire, Université catholique de Louvain, B1348 Louvain-la-Neuve, Belgium*

(Received 10 December 2007; published 20 March 2008)

Rate coefficients for dissociative recombination (DR), dissociative excitation (DE), and vibrational excitation between the helium dimer ion $^4He_2^+$ and electrons from a few meV up to 40 eV were measured using fast (3.8 and 8.3 MeV) ion beams stored for up to 85 s. Vibrational relaxation to greater than 95% in the $v=0$ level was achieved by collisions with cold electrons over 50 s. Low-energy, strongly $v$-dependent DR rate coefficients are given for $v=0$, 1, and $\geq 2$. The rate coefficients at higher energies for $v=0$, with DR and DE given on an absolute scale, are compared to results from recent wave-packet calculations on the fast dissociation dynamics of the doubly excited helium dimer, where the three processes occur as competing reaction channels. Also given are rate coefficients for vibrationally superelastic electron collisions at near 10 meV average energy and the approximate vibrational excitation cross section for fast collisions with the residual gas.

DOI: 10.1103/PhysRevA.77.032719 PACS number(s): 34.80.Lx, 34.80.Ht, 34.80.Gs

## I. INTRODUCTION

The helium dimer ion is an important model system [1] for investigating the electron impact dynamics of small molecular ions and identifying the role of individual vibrational levels and excited potential curves. Moreover, the molecular ion is important in models of the early universe [2] and in helium plasmas and afterglows [3], representing environments where the dissociative recombination (DR) of $He_2^+$ with free electrons is an important destruction mechanism. For a molecular ion with vibrational quantum number $v$ and rotational quantum number $J$, this reaction can be written as

$$He_2^+(v,J) + e^-(E) \rightarrow He(n) + He(n'), \tag{1}$$

where $n$ and $n'$ describe the final states of the neutral atoms, and $E$ is the kinetic energy of the free electron. A further destructive electron collision process of the molecular ion is dissociative excitation (DE), resulting in a neutral helium atom and a helium ion according to

$$He_2^+(v,J) + e^-(E) \rightarrow He(n) + He^+(n') + e^-(E'), \tag{2}$$

where $E'$ is the kinetic energy of the free electron after the collision. Additionally, instead of dissociation, the collision can change the rovibrational state of the molecular ion according to

$$He_2^+(v,J) + e^-(E) \rightarrow He_2^+(v',J') + e^-(E'), \tag{3}$$

where $v'$ and $J'$ are the final vibrational and rotational quantum numbers, respectively, and the process is denoted as rovibrational excitation for $E'<E$ and as superelastic collision (SEC) for $E'>E$. By SEC with low-energy electrons the internal degrees of freedom of a molecular ion may be cooled, as observed earlier for $H_2^+$ [4].

Important potential energy curves and energy levels for the helium dimer ion in the vicinity of the $He_2^+$ ground state are shown in Fig. 1. A remarkable property of this system is that, among the lower vibrational levels $v$ of $He_2^+$, the Franck-Condon overlap with electronically doubly excited potentials of the neutral dimer varies by many orders of magnitude; as illustrated, it is high for $v\geq 3$, but decreases in large steps as $v$ becomes $\leq 2$. At low electron energy, this is responsible for strongly different rates of the various inelastic processes and causes exceptionally low cross sections for the DR of ground state $He_2^+$. Theoretical works [1,7] have confirmed these extremely low DR cross sections between thermal electrons and the $He_2^+$ ion in its lowest rovibrational state, yielding $\sim 10^{-18}$ cm$^2$ for $E\sim 0.03$ eV, resulting in a thermal DR rate coefficient of $\tilde{\alpha}_{DR}(300\ \mathrm{K}) \sim 6 \times 10^{-11}$ cm$^3$ s$^{-1}$, while for excited vibrational levels ($v\geq 3$) the DR cross section is predicted to be larger by four orders of magnitude [1]. At higher electron energies and for higher $v$, also higher doubly excited potential curves below the $A\ ^2\Sigma_g^+$ curve of $He_2^+$ become increasingly important. Their role was analyzed in recent theoretical work where the cross

*henrik.buhr@mpi-hd.mpg.de

†Present address: Department of Physics and Astronomy, University of Aarhus, DK-8000 Aarhus C, Denmark.

‡Present address: CSMP Department, Pacific Union College, Angwin, CA 94508, USA.

§Present address: Columbia Astrophysics Laboratory, Columbia University, New York, NY 10027, USA.

‖Present address: Department of Chemistry, University of California, Berkeley, CA 94720, USA.

¶Present address: Max-Planck-Institut für Quantenoptik, D-85748 Garching, Germany.

 ©2008 The American Physical Society

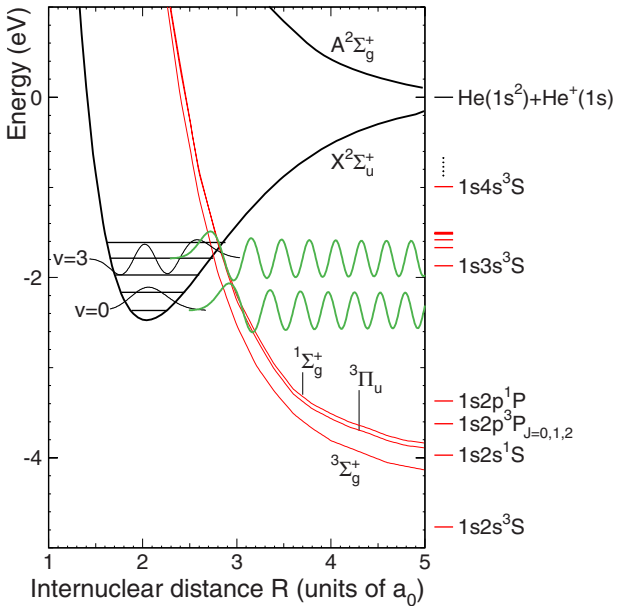


FIG. 1. (Color online) Potential energy curves of $He_2^+$ [5] and the lowest doubly excited potential curves of $He_2$ [6] relevant for low-energy DR. Black thick lines: $He_2^+$ ground state and first excited state with the lowest vibrational levels. Gray (red) thin lines: the lowest doubly excited $He_2$ potential curves. The horizontal lines on the right mark the energies of atomic limits. The thin black lines show qualitatively the wave functions of two bound ionic states of $^4He_2^+$ ($v=0$ and $v=3$), and the thick gray (green) lines show continuum wave functions of the same total energy for the $^3\Sigma_g^+$ dissociative state.

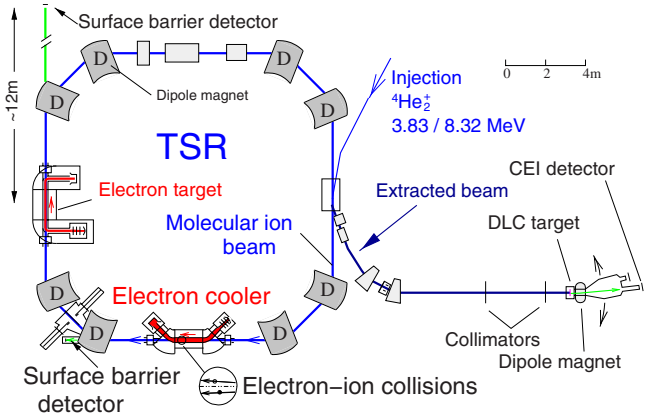


FIG. 2. (Color online) Schematic drawing of the TSR showing the electron cooler with the surface barrier detector downstream, the electron target used for the calibration measurements, and the Coulomb explosion imaging setup with extraction, collimators, and diamondlike carbon (DLC) target [19].

sections for DR, DE, and vibrationally inelastic collisions were calculated for electron energies between 1 and 15 eV in a unified wave-packet approach [8,9].

In recent experiments both the isotopically symmetric $^4He_2^+$ [10] and the asymmetric $^3He\ ^4He^+$ [10,11] have been studied with the merged-beams technique in storage rings. The asymmetric species $^3He\ ^4He^+$ shows vibrational relaxation by spontaneous radiative emission over $\leq 1$ s [11], while this radiative relaxation is absent for $^4He_2^+$. The results for $^3He\ ^4He^+$ ions stored over many seconds [11] showed a strong dependence of the low-energy DR rate on the rovibrational state, spanning several orders of magnitude, in agreement with the theoretical predictions [1]. It was found that the DR signal was dominated by $v \geq 3$, despite a very low population of these states in the stored ion beam [11]. The two experiments performed on $^3He\ ^4He^+$ deduced thermal DR rate coefficients for an electron temperature of 300 K and $v=0$ ions of $3.3(9) \times 10^{-10}$ [11] and $6 \times 10^{-10}$ cm$^3$ s$^{-1}$ [10], respectively. For the higher vibrational states $v \geq 3$, the average rate coefficient was estimated to be $\geq 2 \times 10^{-7}$ cm$^3$ s$^{-1}$ [11]. At higher electron energies, the measured DR rate coefficient for $^3He\ ^4He^+$ showed a broad peak around 7 eV [10,11]. Moreover, smaller peaks in the DR rate were observed above 15 eV [11]; the higher excited potential curves [12] of the $He_2^+$ ion causing these structures are seen in Fig. 2 of Ref. [11]. The data in the only previous experiment on stored $^4He_2^+$ ions [10] showed no signs of vibrational relaxation; the observed vibrationally averaged DR rate coefficient decreased monotonically with increasing electron energy up to ~15 eV and was larger than that of $^3He\ ^4He^+$ for most energies.

In the experiment presented here, we achieved a high degree of vibrational relaxation for stored isotopically symmetric $^4He_2^+$ ions through their interaction with a cold merged electron beam over many seconds. Rate coefficients for DR and DE were then measured as a function of the electron energy up to ~40 eV for ions with greater than 95% population in the vibrational ground state. The vibrational populations were monitored independently of the electron interaction using the method of foil-induced Coulomb explosion imaging described below. The vibrational relaxation is found to be essentially due to SEC, for which experimental rate coefficients for $v=1$ and for $v \geq 2$ are given. Moreover, the energy dependence of vibrational excitation by electrons with energies up to ~30 eV is determined. Significant effects on the DR rate coefficient at low electron energy were also found due to the vibrational heating in collisions of fast $^4He_2^+$ ions with residual gas molecules.

## II. EXPERIMENTAL SETUP AND PROCEDURE

The experiment was performed at the Test Storage Ring (TSR) [13] at the Max-Planck-Institut für Kernphysik in Heidelberg, Germany. A schematic drawing of the storage ring and the detector setup is given in Fig. 2. A $He_2^+$ beam was produced in a duoplasmatron ion source [14] under similar conditions as in Ref. [11]. The ions were accelerated to a kinetic energy $E_i$ of 3.83 or 8.32 MeV, respectively, using a rf accelerator [15] and then injected into the storage ring with circumference $C=55.4$ m, where the beam was stored in the magnetic lattice of dipole and quadrupole magnets. The injection lasted $\leq 40$ $\mu$s and afterward the unbunched ion beam circulated freely in the ring at the injection energy with typical currents of the order of 10 nA. The beam lifetimes $(1/e)$ were limited by collisions with residual gas molecules and amounted to 10 s for $E_i=3.83$ MeV and 15 s for

$E_i$=8.32 MeV, with a residual pressure of (5–10) $\times 10^{-11}$ mbar in the ring.

In one of the straight sections, the ions were merged with a cold electron beam provided by the TSR electron cooler [16] over a length of $L$=1.5 m. The electron beam with ~3 cm diameter was guided by a magnetic field of 0.04 T and the temperatures of the electrons in its comoving reference frame were $kT_\perp$=11.5 meV transverse and $kT_\parallel$ ~0.5 meV parallel to the beam direction. Up to a time of $T_0$=5 s after the injection, the electron velocity was matched to that of the ions. During this time, the electron-ion collisions essentially occur at the electron thermal velocities and, aside from recombination and other inelastic reactions, also lead to translational phase-space cooling (electron cooling) of the stored ion beam, which reduced its diameter to ≤2 mm and its relative momentum spread to $\leq 10^{-4}$ within $T_0$. Moreover, electron-induced collision processes taking place already during this cooling period [17], as well as the other interactions discussed in Sec. II C, lead to changes in the rovibrational populations of the stored ion beam.

Complementary measurements for the absolute calibration of the rate coefficient (see Secs. II B and II D) were performed using the new electron target [18] of the TSR installed in a separate straight section as shown in Fig. 2. It was used with a thermionic cathode, producing an electron beam with a diameter of ~10 mm and electron temperatures of $kT_\perp$=2.8 meV and $kT_\parallel$~0.05 meV in the interaction region. At the given electron and ion beam diameters, the total overlap length of the two beams, including the bent part of the electron beam, was 1.49 m.

### A. Coulomb explosion imaging

The distribution of vibrational levels of the stored molecular ions was determined with the foil-induced Coulomb explosion imaging (CEI) technique as discussed in detail elsewhere [19,20]. Briefly, molecular ions with MeV kinetic energies were slowly extracted from the storage ring into a dedicated beamline (see Fig. 2) where they pass through an ultrathin diamondlike carbon foil (80 Å thickness). Because of the large kinetic energy of the molecular ions, the electrons are stripped very fast, in a much shorter time ($10^{-16}$ s) than the periods of the rotational and vibrational nuclear motions. The trajectories of the two $^4He^{2+}$ nuclei are then essentially determined by the repulsive Coulomb force, and they rapidly reach an asymptotic velocity which depends mainly on the internuclear distance at the moment when the electrons were removed. The kinetic energies $E_k$ released to the resulting $^4He^{2+}$ ions were measured ~3 m downstream from the foil. The distribution of internuclear distances associated with a certain vibrational level $v$ before hitting the stripping foil is thus reflected in a corresponding distribution of measured kinetic energy releases $P_v(E_k)$ that can be modeled accurately [20]. The total normalized distribution of measured kinetic energy releases can then be written as

$$P(E_k,t) = \sum_v p_v(t) P_v(E_k) \quad \text{with} \quad \sum_v p_v(t) = 1, \qquad (4)$$

where $p_v(t)$ is the relative population of a given level $v$ in the stored ion beam at time $t$. The distributions $P_v(E_k)$ were obtained from simulations based on the electronic ground state potential curve of $^4He_2^+$ as given in Ref. [21] following the procedure described in Refs. [11,20,22], accounting for the effects of multiple scattering in the foil and other target and detector effects. Note that the $P_v(E_k)$ distributions are not sensitive to the rotational angular momenta $J$ at least for the typical $J$ values relevant in the present investigation. The vibrational populations $p_v$ can then be extracted from the observed distribution $P(E_k)$ by applying a least-squares fit according to Eq. (4).

### B. Rate measurements

To measure the energy dependence of the DR and DE rate coefficients the relative electron-ion velocity is varied by changing the acceleration voltage of the electron cooler [23]. When the detuning velocity $v_d$ is defined as the difference between the average longitudinal velocities of the electron and the ion beam, the corresponding detuning energy $E_d$ is well approximated by

$$E_d = m_e v_d^2/2, \qquad (5)$$

where $m_e$ denotes the electron mass. The electron-ion collision energies $E$ are nearly monochromatic around $E_d$ except at small $E_d \leq kT_\perp$, where they are given by the finite electron beam temperature.

The detuning energy usually follows, after $T_0$=5 s of electron cooling at $E_d=E_d^c=0$, a cyclic scheme consisting of three different detuning energies: the cooling energy ($E_d^c$), the reference energy ($E_d^r$), and the measurement energy ($E_d^m$). The respective dwell times ($T_c, T_r, T_m$) at the different energies are in the range of 25–125 ms and their ratios are adjusted to the needs of the experiments. The cooling energy $E_d^c$ is applied to preserve the ion beam phase space cooled during all storage times. The energy $E_d^m$ defines the detuning energy at which the DR and DE rates are to be determined. For normalization purposes the DR and DE rates are also measured at a fixed reference energy $E_d^r$.

As the electron beam current is a monotonically increasing function of the electron acceleration voltage, the electron density $n_e$ depends on the detuning energy $E_d$. In the present experiment, the measurement energies $E_d^m$ as well as the reference energies $E_d^r$ are reached by applying positive velocity differences $v_d$ corresponding to an electron beam moving faster than the ion beam; thus, the density $n_e(E_d)$ is increasing with $E_d$. Moreover, higher ion beam energies $E_i$ go along with higher electron acceleration voltages at matched beam velocities ($E_d=E_d^c=0$), so that the respective electron densities at cooling, $n_e(E_d^c)$, increase with $E_i$. Experiments were performed at two distinct sets of operating parameters, denoted as type A and type B. The corresponding ion beam energies $E_i$, electron densities $n_e(E_d^c)$, as well as the energies $E_d^r$ chosen for the reference step are listed in Table I. The two sets differ in particular with respect to the electron density; the density was changed by a factor of 2 in order to study the excitation of the stored ions by electron collisions. Absolute values for the electron beam densities $n_e$ are determined from the measured electron currents using the electron beam size and its density profile, known with a relative accuracy of 10%.

TABLE I. Ion and electron beam parameters for the two measurement schemes, differing by the ion energy $E_i$, the electron density during cooling, $n_e(E_d^c)$, and the detuning energy $E_d^r$ used to collect a reference signal.

| | $E_i$ (MeV) | $n_e(E_d^c)$ ($10^6$ cm$^{-3}$) | $E_d^r$ (eV) |
|---|---|---|---|
| Type A | 3.83 | 5.5 | 7.3 |
| Type B | 8.32 | 11 | 23.5 |

Neutral fragments emerging from electron-ion collisions as well as rest-gas collisions are separated from the ion beam at the bending dipole magnet following the electron cooler and impact on an energy-sensitive $40\times60$ mm$^2$ Si surface barrier detector and are recorded with a detector efficiency of 100%. Signals corresponding to half (full) energy of the stored $^4He_2^+$ ions are due to the detection of only one (mass 4) [both (mass 8)] neutral He fragments and are observed with rates denoted by $R_{(4)}(E_d)$ and $R_{(8)}(E_d)$, respectively. The large size of the Si detector and its moderate distance from the center of the electron cooler ensure that the dissociation cones due to DR and DE events are within the detector acceptance even for the largest detuning energies $E_d$.

The measurements of the energy dependence of the DR and DE rate coefficients were performed using the following procedure. For a given injection the rates $R_{(k)}(E_d^j)$ $(k=4,8, j=c,m,r)$ were measured for a fixed $E_d^m$ value by cycling through the three energies $E_d^c$, $E_d^m$, and $E_d^r$ with dwell times $T_c$, $T_r$, and $T_m$ for an interval of storage times $t$ ranging from $T_0=5$ s up to the end of storage at 85 s at a maximum. The detuning energy $E_d^m$ was then varied from injection to injection until the selected scan range of $E_d^m$ values was covered. These scans were repeated a number of times until a sufficient statistical accuracy of the rates $R_{(k)}(E_d^j)$ could be achieved when averaging them over all scans. From these rates the energy- and storage-time-dependent rate coefficients for the DR and DE process can be deduced as discussed in Sec. II E.

### C. Rest-gas-induced processes

As already pointed out in the Introduction, the low-energy DR rate coefficient of $He_2^+$ is known to vary strongly with its vibrational excitation [1,11]; hence, even small changes in the internal excitation of the ions will influence the observed low-energy DR rate coefficient. It is therefore important to consider also all other types of collision processes which may affect the rovibrational population of the ions stored in the ring besides those induced by collisions with the free electrons of the electron cooler. Moreover, these additional processes may contribute to the measured rates $R_{(k)}(E_d^j)$ and eventually have to be taken into account.

While interactions with the ambient radiation field are negligible because of the vanishing dipole moment of $^4He_2^+$, collisions of the stored $He_2^+$ ions with molecules $R$ of the residual gas, composed mostly of $H_2$, have to be considered more carefully. Possible reaction channels are dissociative excitation (DE-$R$),

$$He_2^+(v,J) + R \rightarrow He + He^+ + R, \tag{6}$$

dissociative charge exchange (DC-$R$),

$$He_2^+(v,J) + R \rightarrow He + He + R^+, \tag{7}$$

and inelastic processes (IE-$R$) resulting in excitations or deexcitations,

$$He_2^+(v,J) + R \rightarrow He_2^+(v',J') + R. \tag{8}$$

Because the relative energy between the $He_2^+$ ions and the rest gas is much larger than their internal excitation energy, it is safe to assume that neither the DE-$R$ nor the DC-$R$ cross section depends on the internal excitation of the $He_2^+$ ions. Rovibrational excitation in collisions with the residual gas due to the IE-$R$ process, however, cannot be neglected and will be discussed in more detail in Sec. III E.

While the IE-$R$ process is nondestructive, both the DC-$R$ and DE-$R$ process may contribute to the measured rates $R_{(8)}$ and $R_{(4)}$, respectively. Rate measurements performed with the electron beam turned off revealed, however, that the DC-$R$ rates are small and only of the order of $\sim$1% of the DE-$R$ rate. On the other hand, the finite DE-$R$ cross section and its insensitivity to the internal excitation of the $^4He_2^+$ ions do allow use of the rates $R_{(4)}(E_d^c,t)$ recorded at the cooling energy $E_d^c$ as a monitor for the number of ions stored at time $t$, the electron-induced DE not being able to contribute at $E_d^c=0$ because of the finite threshold of $\sim$2.4 eV for this process [21].

### D. Absolute calibration of the rate coefficient scales

To obtain an absolute scale for the rate coefficients, the absolute DR rate coefficient for $v=0$ $^4He_2^+$ ions at $E_d^{abs}=7.4$ eV was determined in a separate measurement, which was performed using the electron target and applying a method similar to that described in Ref. [11]. In short, this technique exploits the difference in lifetimes of the ion beam and the differences between the absolute count rates $R_{(4)}$ and $R_{(8)}$ when the electron beam tuned at $E_d^{abs}$ is switched on and off. The method assumes that the shortening of the beam lifetime observed when the electron beam is switched on is exclusively due to the electron-induced DR and DE processes or due to changes of the DE-$R$ or DC-$R$ processes caused by the presence of the electron beam, which are both reflected by the observed rates $R_{(4)}$ and $R_{(8)}$. Slight changes of the rest-gas-induced processes DE-$R$ or DC-$R$ are expected to arise from slow residual gas ions generated by the electron beam and radially confined in its space charge field, whose density is kept below a few percent of the electron density by suitable extraction fields downstream of the interaction region. The measurement was performed after 30 s of intense electron cooling. In fact, as shown by Fig. 3 under conditions of weaker electron-induced vibrational cooling (type A), the rate coefficient is found to be stationary at this energy already for storage times larger than 15 s. Thus, the DR rate determined in this calibration measurement can be assumed to be essentially given by that of the vibrationally relaxed $^4He_2^+$ ions.

The absolute DR rate coefficient resulting from this measurement (using the notation introduced in Sec. II E) is

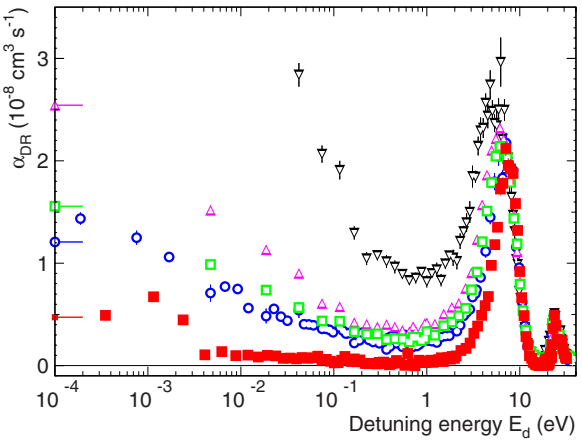


FIG. 3. (Color online) Effective DR rate coefficient as a function of the detuning energy $E_d$ for storage time slices of 7–14 s (downward triangles), 22.5–45 s (upward triangles), 33.75–58 s (open squares), and 54–85 s (circles). In addition to these results obtained with type-A parameters, the result from a type-B experiment and storage times >58.5 s is also shown (filled squares). Dwell-time ratios during the measurement are $T_c:T_r:T_m=1:1:4$. In the given range the toroid correction (Sec. II E) is largest for detuning energies of $E_d=1-5$ eV, where it amounts to $\Delta\alpha_{DR}=(0.1-0.2)\times10^{-8}$ cm$^3$ s$^{-1}$.

$\alpha_{DR}^{abs}(E_d^{abs})=2.0(1)(4)\times10^{-8}$ cm$^3$ s$^{-1}$, where the first value in parentheses represents the statistical and the second the systematic error. The main contribution to the systematic uncertainty stems from the electron density.

### E. Effective rate coefficients

Correcting the measured rates $R_{(8)}(E_d^m,t)$ and $R_{(4)}(E_d^m,t)$ (see Sec. II B) for rest-gas-induced contributions, and normalizing them to the electron density as well as to the number of stored ions, relative *effective* rate coefficients $\tilde{\alpha}(E_d^m,t)$ for the DR and DE processes can be deduced, i.e., rate coefficients which are *averaged* over the rovibrational states populated at the time $t$ when the rate measurement took place.

As a measure for the number of stored particles at time $t$, the rates $R_{(8)}(E_d^r,t)$ and $R_{(4)}(E_d^c,t)$ recorded during the reference or cooling intervals ($T_r$ and $T_c$) directly preceding the measurement interval $T_m$ can be used. As discussed in Sec. II C for the $R_{(4)}(E_d^c,t)$ rates, and for the $R_{(8)}(E_d^r,t)$ rates at $E_d^r$ energies of 7.3 and 23.5 eV in Sec. III A, both rates are essentially independent of the internal excitation of the molecular ions. Indeed they show, up to a constant factor, the same dependence on the storage time $t$. As the rates $R_{(4)}(E_d^c,t)$ were usually much higher than those at the reference energies, the $R_{(4)}$ rates at cooling energy were finally used as the measure for the number of stored ions.

Relative rovibrationally averaged DR rate coefficients were thus obtained by

$$\tilde{\alpha}_{DR,r}(E_d^m,t)=\frac{1}{n_e(E_d^m)}\frac{R_{(8)}(E_d^m,t)}{R_{(4)}(E_d^c,t)} \tag{9}$$

and the corresponding DE rate coefficient by

$$\tilde{\alpha}_{DE,r}(E_d^m,t)=\frac{1}{n_e(E_d^m)}\left(\frac{R_{(4)}(E_d^m,t)}{R_{(4)}(E_d^c,t)}-\epsilon\right). \tag{10}$$

Here, the constant parameter $\epsilon$ describes the residual-gas-induced background rate per ion; it can be neglected for the DR channel (see also Sec. II C), while for the DE channel it is adjusted such that the DE rate coefficient averages to zero below the threshold (2.37 eV for $v=0$ $^4He_2^+$ ions [21]).

The energy-dependent relative rate coefficients were then corrected for contributions from electron collisions occurring at higher energies in the two merging regions (toroidal magnetic field regions) of the electron and ion beams. These toroidal contributions, mostly appearing as additional broad structures on the low-energy side of threshold or pronounced peak features, were deconvoluted in an iterative procedure [24] yielding corrected relative rate coefficients $\tilde{\alpha}_{DR,r}^{tc}(E_d^m,t)$ and $\tilde{\alpha}_{DE,r}^{tc}(E_d^m,t)$ after small corrections illustrated in Sec. III A.

Finally, absolute effective DR and DE rate coefficients were obtained by normalizing the relative, toroid-corrected rate coefficients to the absolute DR rate coefficient measured for $v=0$ $^4He_2^+$ ions at $E_d^{abs}=7.4$ eV as described in Sec. II D. It is considered safe to assume that at these high detuning energies the DR rate coefficient is largely independent of the rotational population of the $^4He_2^+$ ions, so that only *vibrationally* cold ions are required for a valid normalization. Hence, using a reference rate coefficient $\tilde{\alpha}_{DR,r}^{tc,v=0}(E_d^{abs})$ obtained at $E_d^m=E_d^{abs}$ and in a suitable storage time interval ensuring a vibrationally cold ion beam, both the effective DR and the DE rate coefficient can be obtained on the absolute scale by

$$\tilde{\alpha}_{DR}(E_d^m,t)=\tilde{\alpha}_{DR,r}^{tc}(E_d^m,t)\frac{\alpha_{DR}^{abs}(E_d^{abs})}{\tilde{\alpha}_{DR,r}^{tc,v=0}(E_d^{abs})} \tag{11}$$

and

$$\tilde{\alpha}_{DE}(E_d^m,t)=\tilde{\alpha}_{DE,r}^{tc}(E_d^m,t)\frac{\alpha_{DR}^{abs}(E_d^{abs})}{\tilde{\alpha}_{DR,r}^{tc,v=0}(E_d^{abs})} \tag{12}$$

at arbitrary storage times $t$ and detuning energies $E_d^m$.

All absolute rate coefficients given in this work are obtained using this calibration procedure and are quoted with their statistical errors only; they carry an additional systematic uncertainty of ±20% according to the error estimate for $\alpha_{DR}^{abs}(E_d^{abs})$ given in Sec. II D.

### F. Vibrational-state-specific DR rate coefficients

The measured rate coefficients discussed above are effective values representing averages over all initial rovibrational states $v,J$ of the molecular ions populated at time $t$. Therefore, denoting the relative populations by $p_{vJ}(t)$, the effective DR rate coefficients can be expressed by

$$\tilde{\alpha}_{DR}(E_d,t)=\sum_{vJ}p_{vJ}(t)\alpha_{DR}^{(vJ)}(E_d), \tag{13}$$

where $\alpha_{DR}^{(vJ)}$ denotes the DR rate coefficient for a specific state $v,J$ and $\Sigma p_{vJ}(t)=1$. As described in Sec. II A, the Coulomb explosion imaging method allows the vibrational level

populations $p_v(t)=\Sigma_J p_{vJ}(t)$ to be measured. Using this information, the measured rate coefficient can be decomposed at least in terms of vibrational-state-specific, but still $J$-averaged, rate coefficients:

$$\tilde{\alpha}_{\mathrm{DR}}(E_d,t)=\sum_v p_v(t)\tilde{\alpha}_{\mathrm{DR}}^{(v)}(E_d). \tag{14}$$

Note that the available theoretical calculations [1] suggest that for $He_2^+$, especially among the levels $v\leq 3$, the rotational dependence is much weaker than the vibrational dependence even at very low detuning energies.

Using CEI results for the vibrational populations $p_v(t_i)$ at specific times $t_i$ $(i=1,\ldots,N)$ and a corresponding set of measured rate coefficients $\tilde{\alpha}_{\mathrm{DR}}(E_d,t_i)$, vibrational-state-specific rate coefficients $\tilde{\alpha}_{\mathrm{DR}}^{(v)}(E_d)$ can be extracted for individual $v$ levels from the $N$ corresponding linear equations derived from Eq. (14).

## III. RESULTS

### A. Energy and storage-time dependence of DR

The basic dependence of the DR rate coefficient on the detuning energy $E_d^m$ between the electron and the ion beam and on the storage time $t$ is shown in Fig. 3. Here, $E_d$ is modulated as described in Sec. II B at storage times $t>5$ s with a dwell-time ratio of $T_c:T_r:T_m=1:1:4$. This allows us to monitor the temporal evolution of the stored $^4He_2^+$ beam through the detected energy-dependent count rates for $t>5$ s. Already for the lowest storage time interval of $t=7-14$ s, DR mainly occurs in two energy regions, at $E_d\leq 0.1$ eV and in a broad peak at $E_d\sim 2.5-12.5$ eV. We interpret the low-energy DR, especially at shorter storage times, as originating mainly from ions in vibrational states with $v\geq 3$ showing good Franck-Condon overlaps with the lowest doubly excited $He_2$ potential, while the high-energy peak arises from vibrationally relaxed ions $(v\leq 2)$ for which a good Franck-Condon overlap with doubly excited $He_2$ potentials is reached only at higher collision energy. The low-energy component continues to decrease over the later storage times (up to $t\sim 60$ s), showing indications of a low-lying resonance structure near $10^{-3}$ eV. The high-energy component up to detuning energies below 7 eV changes mainly over the interval of $t\leq 20$ s, indicating that a large fraction of ions are in the $v=0$ vibrational state already after this storage time, while the DR rate coefficients above 7 eV are basically time independent over the whole span of storage times measured.

These data indicate very significant vibrational cooling of the stored $^4He_2^+$ beam in spite of the absence of spontaneous radiative relaxation. The energy dependence of the DR rate coefficient found by this time-slicing method is in strong contrast with those observed in the only previous storage ring DR experiment [10] on $^4He_2^+$, which will be discussed in more detail in Sec. IV B.

### B. Vibrational relaxation

In order to explore the vibrational relaxation of the stored $^4He_2^+$ ion beam in more detail, the time dependence of the effective DR rate coefficient $\tilde{\alpha}_{\mathrm{DR}}(0,t)$ at matched beam velocities, i.e., for $E_d^m=0$, was observed for varying electron densities and dwell-time ratios. The influence of the electron densities used in the experimental parameter sets types A and B (Table I) is shown in Fig. 4. The electron densities of the two parameter sets differ by a factor of 2, which is expected to enhance vibrational cooling through electron-induced processes [Eqs. (1) and (3)] for type B. The dwell-time ratios were set to $T_c:T_r:T_m=5:1:0$.

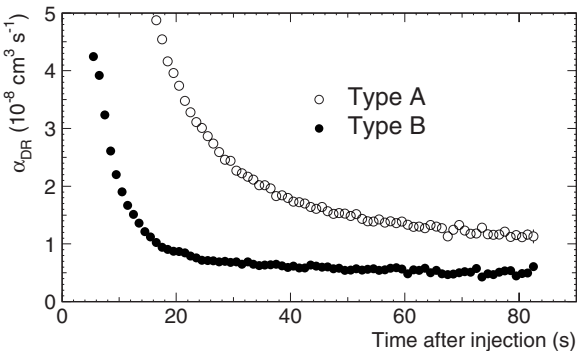


FIG. 4. Effective DR rate coefficient at $E_d=0$ as a function of storage time at low (type-A parameters, open dots) and high (type-B parameters, filled dots) electron density, and dwell-time ratios of $T_c:T_r:T_m=5:1:0$.

In both cases, $\tilde{\alpha}_{DR}$ is seen to decrease rapidly with time, the decrease being much faster for the case of high electron density (type B). For type-A parameters, the time dependence of the relaxation is consistent with that found in Fig. 3 at $E_d^m=0$ (see marks on the left-hand axis of Fig. 3), where for dwell-time ratios of 1:1:4 the fraction of time over which the ion beam is exposed to low-energy electrons assumes the same value of 5/6 as in Fig. 4. Based on the expected strong dependence of the DR rate coefficient on $v$, the variation of $\tilde{\alpha}_{\mathrm{DR}}(0,t)$ is interpreted as due to the cooling of the internal excitation of the molecular ions, primarily of the vibrations. Even for the fast initial cooling realized in the type-B experiment, the DR signal continues to decrease slightly over the full measuring time, showing that variations of the rovibrational population still occur on a time scale of 50–100 s.

A direct determination of the vibrational populations in the stored $^4He_2^+$ ion beam was performed using the CEI method (Sec. II A). In these measurements the ion beam was continuously merged with the electron beam at $E_d=0$, corresponding to dwell-time ratios of $T_c:T_r:T_m=1:0:0$. At times $t_i=5$, 7, 10, 12.5, 15, 17.5, 22.5, and 50 s, the electron beam was switched off and the molecular ions were slowly extracted from the ring into the CEI beamline (Fig. 2). Possible influences of vibrational excitation by the residual gas (studied separately as described below) during the CEI measurement at $t>t_i$ were kept at a negligible level by limiting the CEI data-taking period to the first 7 s after switching off the electron beam. The results of the CEI analysis are shown in Fig. 5. After the time $T_0=5$ s spent for precooling, all $v\geq 2$ vibrational states are already populated by less than 20%. About 15 s after the injection, the ion beam consists almost completely of molecules in the vibrational states $v=0$ and 1. Finally, after 50 s of storage and electron cooling,

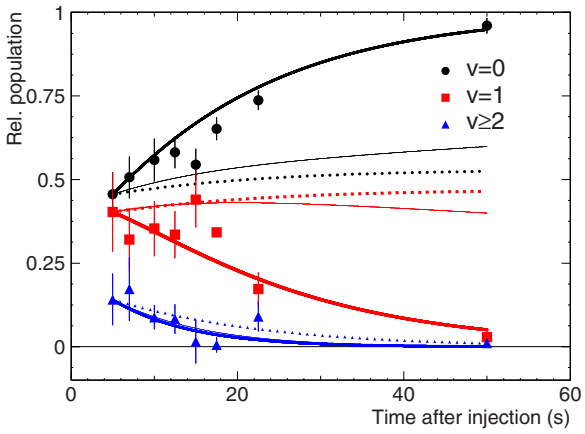


FIG. 5. (Color online) Temporal evolution of the vibrational state distribution in the stored $^4He_2^+$ ion beam measured with the CEI technique as a function of the time $t_i$ spent with electron cooling using type-B parameters. Relative populations are shown for $v=0$ (circles), $v=1$ (squares), and the sum of all other contributions, $v\geq 2$ (triangles). Model calculations neglecting SEC (broken and full thin curves) and including SEC (full thick curve) are also shown; these will be discussed in more detail in Sec. III F.

the vibrational ground state dominates the population with a contribution of ~97%. The origin of the observed cooling will be discussed in more detail in Sec. III F.

### C. High-energy DR and DE rate coefficients

Results of dedicated measurements on the high-energy resonances from the DR of $^4He_2^+$ ions are shown in Fig. 6. Within the injection cycles, the data were obtained after full

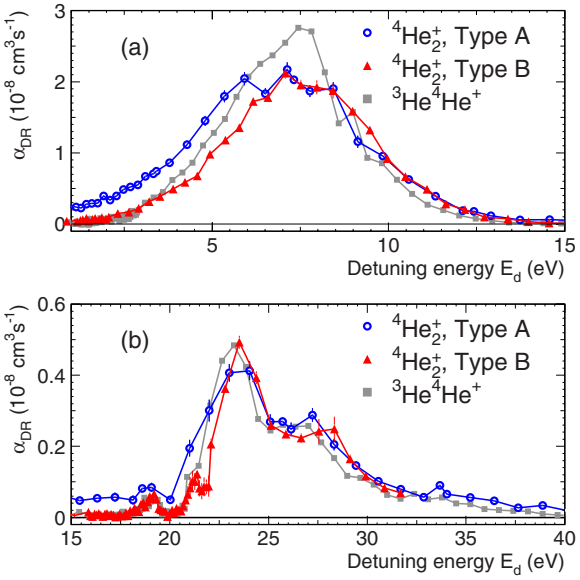


FIG. 6. (Color online) Effective high-energy DR rate coefficient $\tilde{\alpha}_{DR}(E_d)$ for $^4He_2^+$ at detuning energies $E_d<15$ eV (a) and $E_d>15$ eV (b), as measured in the present experiment for type A, $t>54$ s (circles), and type B, $t>58.5$ s (triangles). The rate coefficients are compared to previous results obtained for $^3He\ ^4He^+$ (small squares, Ref. [11], at $t=35-68$ s).

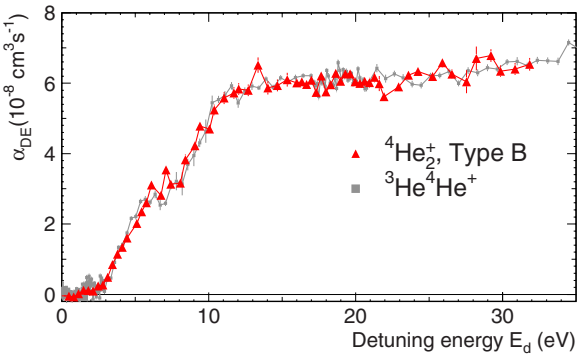


FIG. 7. (Color online) Effective DE rate coefficient $\tilde{\alpha}_{DE}(E_d)$ for $^4He_2^+$ as measured in the present type-B experiment, $t>58.5$ s (triangles). For comparison, the DE rate coefficient determined in Ref. [11] for $^3He\ ^4He^+$ (multiplied by a factor of 2 as discussed in the main text) is shown by the small squares.

electron cooling ($T_c:T_r:T_m=1:0:0$) up to the given starting time of the measurement, which was then performed with dwell times of $T_c:T_r:T_m=1:1:4$. Among the two results shown for $^4He_2^+$, the data for type A (corresponding to a lower electron density) are somewhat broader toward lower energies than those for type B, which leads us to suspect a slight degree of vibrational excitation for the type-A data. On the other hand, for type B, according to the vibrational populations from Fig. 5, less than 5% of the stored ions should be in $v\geq 1$. The structures are largely similar to those observed at the earlier TSR experiment on $^3He\ ^4He^+$ [11] and will be compared in more detail in Sec. IV.

We have also obtained the DE rate coefficient of $^4He_2^+$, which is shown in Fig. 7 for the type-B parameters implying <5% population in $v\geq 1$. The DE rate coefficient of $^3He\ ^4He^+$ is plotted for comparison. As the DE rate coefficient was determined in Ref. [11] only for the $^4He^+ + ^3He$ channel, we multiplied the result given there by a factor of 2 to account also for the $^4He + ^3He^+$ channel. For completeness we point out that the measured rates of the channels $^4He + ^3He^+$ and $^3He + ^4He^+$ were of the same size within the statistical errors (down to ~5%) in the measurements reported in Ref. [11].

### D. Vibrational-level-specific low-energy DR rate coefficients

Inserting the time-dependent CEI data of Fig. 5 and the DR data of Fig. 4 (type B) into Eq. (14) allows us to extract the vibrational-state-specific DR rate coefficients at $E_d=0$, $\tilde{\alpha}_{DR}^{(v)}(0)$, as described in Sec. II F. In order to ensure that the effective electron cooling time with the dwell-time ratios of $T_c:T_r:T_m=5:1:0$ in the rate coefficient measurement was the same as in the CEI measurement with ratios of 1:0:0, the relative populations determined by CEI at time $t_i$ were combined with the rate coefficients $\tilde{\alpha}_{DR}(E_d,t_i')$ observed at time $t_i'=5\ \text{s}+(6/5)(t_i-5\ \text{s})$. Effects of vibrational heating by electrons at the reference energy $E_d^r$ can be neglected in the case of type-B parameters, as shown in Sec. III E.

Values are deduced for the vibrational-level-specific low-energy DR rate coefficients for $v=0$, $v=1$, and $v\geq 2$ as given in Table II. Note that the constant level found at long storage

TABLE II. Vibrational-level-specific low-energy DR rate coefficients and thermal DR rate coefficients for the low-lying levels of $^4He_2^+$ derived from time-dependent DR rate measurements and the vibrational populations from CEI.

| Vibrational state | $\tilde{\alpha}_{DR}^{(v)}(0)$ ($10^{-9}$ cm$^3$ s$^{-1}$) | $\tilde{\alpha}_{DR}^{(v)}(300\ K)$ ($10^{-9}$ cm$^3$ s$^{-1}$) |
|---|---|---|
| 0 | $3.4 \pm 2.0$ | $1.7 \pm 1.0$ |
| 1 | $3.2^{+17.8}_{-3.2}$ | $1.6^{+8.7}_{-1.6}$ |
| $\geq 2$ | $202^{+153}_{-62}$ | $99^{+75}_{-30}$ |

times and strong relaxation for the vibrationally averaged rate $\tilde{\alpha}_{DR}(0)$ in Fig. 4 amounts to $5.0(4) \times 10^{-9}$ cm$^3$ s$^{-1}$, which results in an upper limit for the $v=0$ rate coefficient when full vibrational relaxation is assumed.

Assuming that the low-energy DR cross sections vary in inverse proportion to the interaction energy, the results obtained for $\tilde{\alpha}_{DR}^{(v)}(0)$ can be converted to thermal DR rate coefficients $\tilde{\alpha}_{DR}^{(v)}(300\ K)$, taking into account the merged-beam electron temperatures [11]. The present results obtained for $v=0$ and 1 (see Table II) are compatible with the thermal rate coefficients of several $10^{-10}$ cm$^3$ s$^{-1}$ previously found for $^3$He $^4$He$^+$ [11]. On the other hand, the thermal rate coefficients for $v \geq 2$ reach the order of magnitude of $\sim 10^{-7}$ cm$^3$ s$^{-1}$, similarly to the earlier findings [11] for $v \geq 3$ in $^3$He $^4$He$^+$.

### E. Vibrational excitation

The constant value of the effective low-energy DR rate coefficient reached at long storage times appears to reflect a steady state between electron-induced rovibrational cooling and counteracting heating processes, maintaining a population of excited vibrational levels sensitively detected through the highly $v$-dependent low-energy DR rate of $He_2^+$. This is demonstrated by Fig. 8 where, for relatively weak cooling

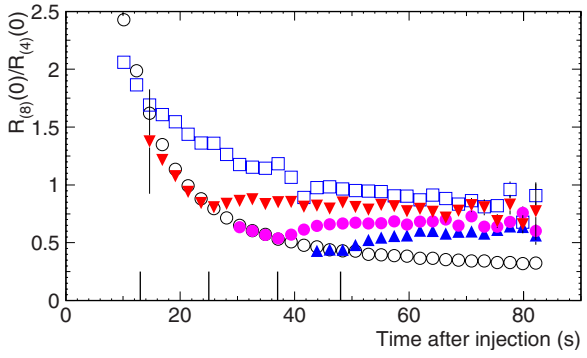


FIG. 8. (Color online) Effective DR rate coefficient at $E_d=0$ as a function of storage time for the experimental parameters of type A with initial dwell-time ratios of $T_c:T_r:T_m=5:1:0$ changed to 1:2:0 at one of the times marked. Open circles show the rate with the dwell-time ratios kept at their initial values, corresponding to the type-A data of Fig. 4, while the results for switching times of 13, 25, 37, and 48 s are shown by open squares, downward triangles, filled circles, and upward triangles, respectively.

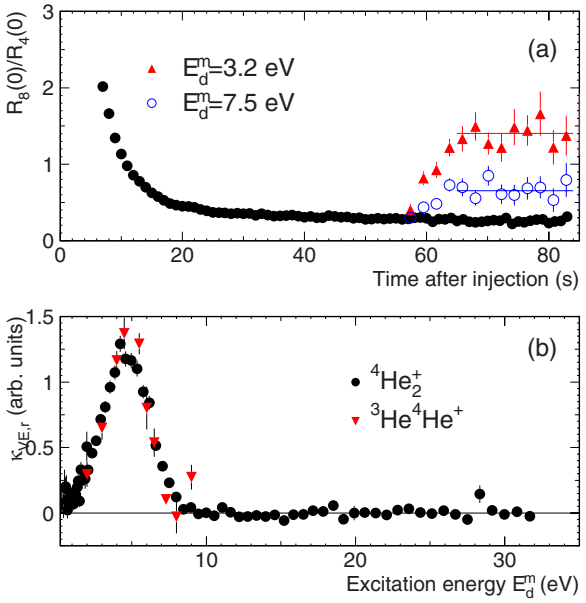


FIG. 9. (Color online) Measurements of the energy dependence of inelastic electronic collision rates. (a) Rate ratio $R_{(8)}(0)/R_{(4)}(0)$ proportional to the effective low-energy DR rate coefficient $\tilde{\alpha}_{DR}(E_d^c,t)$ during the cooling interval $T_c$ for $T_c:T_r:T_m=5:1:0$ (filled circles), corresponding to the type-B data of Fig. 4. These ratios are compared to results obtained when the dwell-time ratios changed to 1:1:4 at $t=54$ s, applying measurement energies $E_d^m$ of 3.2 (upward triangles) and 7.5 eV (open circles), respectively. The lines show the average rate ratio between 65 and 84 s used to derive the energy dependence of the inelastic collision rate. (b) Vibrational excitation functions $\kappa_{VE,r}(E_d^m)$ using Eq. (15) for $^4He_2^+$ (circles) and the data of Ref. [11] for $^3$He $^4$He$^+$, derived as discussed in the main text and scaled to the $^4He_2^+$ data (downward triangles).

(type A), the dwell-time ratios were changed at various storage times. In all cases, the rate coefficient is seen to change its temporal behavior at the time when the dwell-time ratios are switched, and to approach a higher, asymptotic level that is independent of the time of this switching.

The observation of a steady-state DR rate $R_{(8)}(0)/R_{(4)}(0)$ [cf. Eq. (9)] varying with the applied dwell-time ratio, i.e., with the relative time over which the ions interact with low-energy electrons, clearly indicates the presence of excitation processes transferring the stored ions into higher vibrational states, which then lead to higher low-energy recombination rates. Possible mechanisms for such processes are rovibrationally inelastic collisions by electrons at elevated interaction energy $E$, Eq. (3), or inelastic residual-gas collisions according to Eq. (8).

Rovibrationally inelastic electronic collisions have been identified by detecting the low-energy rate coefficient $\tilde{\alpha}_{DR}(E_d^c,t)$ during the cooling interval $T_c$ of the energy modulation cycle (Sec. II B) while causing excitation by electrons at $E_d^m$ during the measurement interval $T_m$. In this series of measurements a distinct rise of the measured low-energy rate $R_{(8)}(0)/R_{(4)}(0)$, proportional to the rate coefficient $\tilde{\alpha}_{DR}(0)$, to a new constant level is seen after applying the electron excitation at $t>58$ s [Fig. 9(a)]. Since $\tilde{\alpha}_{DR}(0)$ is sensitive to the population in high-$v$ levels, especially $v \geq 2$, we interpret this as the effect of vibrational excitation. Combining the

heating during $T_m$ and the cooling during $T_c$, a new equilibrium value of $R_{(8)}(0)/R_{(4)}(0)$ is reached. The significant dependence of this equilibrium on $E_d^m$ indicates an important contribution from vibrational excitation (VE) by electron collisions.

We denote the energy dependence of the electron-induced change in $R_{(8)}(0)/R_{(4)}(0)$, normalized to the electron density $n_e(E_d^m)$ at excitation, as the excitation function $\kappa_{\mathrm{VE,r}}(E_d^m)$. It is obtained from the difference $\Delta[R_{(8)}(0)/R_{(4)}(0)]$ between the new equilibrium signal and its initial level as

$$\kappa_{\mathrm{VE,r}}(E_d^m) = \frac{1}{n_e(E_d^m)}\left[\Delta\left(\frac{R_{(8)}(0)}{R_{(4)}(0)}\right) - \epsilon'\right]. \tag{15}$$

$\epsilon'$ accounts for small contributions in the measured rise that stem from the change of the dwell-time ratios in the presence of other heating processes unrelated to the electrons at $E_d^m$. Since no dependence of the equilibrium level on the electron energy is observed at $E_d^m > 10$ eV, we assume that excitation by electron collisions becomes inefficient above this energy and choose $\epsilon'$ so that the average value of $\kappa_{\mathrm{VE,r}}(E_d^m)$ becomes zero there. The observed excitation function $\kappa_{\mathrm{VE,r}}(E_d^m)$ for $^4He_2^+$ is shown in Fig. 9(b). It shows a clear peak extending from 1 to 8 eV with a maximum at $E_d^m \sim 4.5$ eV; the subtracted offset $\epsilon'$ is about 30% of $\Delta[R_{(8)}(0)/R_{(4)}(0)]$ at the peak maximum.

The function $\kappa_{\mathrm{VE},r}(E_d^m)$ measured by this method must be interpreted with caution. Considering only $v=0$ for the initial population and denoting the final levels by $v'$, it is related to the individual vibrational excitation rate coefficients $\tilde{\alpha}_{\mathrm{VE}}^{(0\to v')}(E_d^m)$ by

$$\kappa_{\mathrm{VE},r}(E_d^m) = C_\kappa \sum_{v'>0} \tilde{\alpha}_{\mathrm{VE}}^{(0\to v')}(E_d^m)\tilde{\alpha}_{\mathrm{DR}}^{(v')}(0), \tag{16}$$

where $C_\kappa$ denotes an absolute normalization constant unspecified here. Thus, the observed effect includes a $v'$-dependent weighting of the excitation rate. However, if the energy dependences of $\tilde{\alpha}_{\mathrm{VE}}^{(0\to v')}(E_d^m)$ are similar among the different $v'$, their common energy dependence is approximately given by $\kappa_{\mathrm{VE},r}(E_d^m)$ and the weighting by $v'$ modifies only the overall normalization. For the approximate interpretation of the features observed here we assume such a common energy dependence, as they lie substantially above the vibrational excitation thresholds of $He_2^+$.

Data from the previous experiment on $^3$He $^4$He$^+$ are included for comparison. Here, the fraction of high-$v$ $^3$He $^4$He$^+$ ions has been identified through the measured part $N_d^{\mathrm{R1}}$ of fragment-imaging events with small energy release (region R1) in Fig. 19(b) of Ref. [11] as a function of the excitation energy $E_d^m$. To derive the excitation function $\kappa_{\mathrm{VE,r}}(E_d^m)$, we again subtract an offset estimated to cause a zero signal for $E_d^m > 10$ eV and normalize to $n_e(E_d^m)$. Both excitation functions are scaled arbitrarily by independent factors for the comparison in Fig. 9(b), which shows that their energy dependences are very similar.

Basically, the absolute size of the vibrational excitation rate coefficients can be inferred from the population changes caused by the excitation signal as, in the analyzed equilibrium levels, the relative change in these populations represents the ratio of the vibrational excitation rate to the cooling rate. However, these populations can be estimated only roughly because of the incomplete knowledge of the $v$ levels reached by the excitation process and of the individual rate coefficients $\tilde{\alpha}_{\mathrm{DR}}^{(v)}(0)$. For $^4He_2^+$, considering the single value for $v \geq 2$ from Table II together with the observations on vibrational heating in the residual gas discussed below (Fig. 10), the observed increase in $R_{(8)}(0)/R_{(4)}(0)$ [using the relaxed value of $\tilde{\alpha}_{\mathrm{DR}}(0)$ from Fig. 4] indicates an electron-induced excited population amounting to about 3% on the excitation peak. Accordingly, the excitation rate is of the order of 3% of the vibrational cooling rate. The latter is caused dominantly by low-energy electron collisions, for which (at higher $v$) a rate coefficient in the upper $10^{-7}$ cm$^3$ s$^{-1}$ range is derived (Sec. III F). With the given equilibrium population, the rate coefficient at the maximum of the excitation curve is then estimated to lie in the low $10^{-8}$ cm$^3$ s$^{-1}$ range.

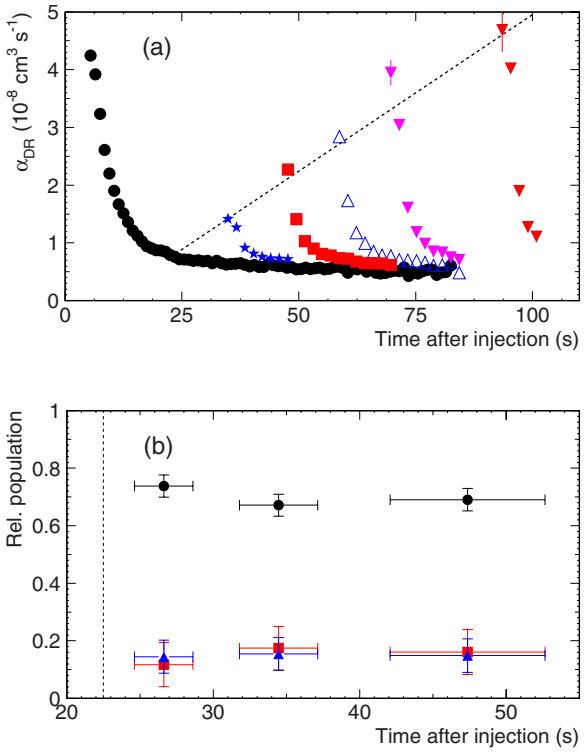


FIG. 10. (Color online) Measurements on vibrational heating in ion–residual-gas collisions. (a) Effective low-energy DR rate coefficient $\tilde{\alpha}_{\mathrm{DR}}(E_d^c, t)$ $(E_d^c=0)$ for $T_c:T_r:T_m=5:1:0$ (filled circles), corresponding to the type-B data of Fig. 4, compared to results with the electron beam switched off at $t=t_{\mathrm{off}}=22.5$ s and switched back on after off times of 11 (asterisks), 22.5 (squares), 34 (upward triangles), 45 [downward light (magenta) triangles], and 67.5 s [downward dark (red) triangles]. The dashed line starting at 22.5 s is to guide the eye along the onset points of the individual measurements. (b) Relative populations of the $v=0$ (circles), $v=1$ (squares), and $v \geq 2$ (triangles) vibrational levels measured with the CEI technique; full electron cooling (type-B parameters) is switched off at $t_{\mathrm{off}}$ (dashed vertical line) and the CEI measurement is extended over an interval which is marked by the average time and the rms of the times of the single events.

For $^3$He $^4$He$^+$, the detected signal $N_d^{R1}$ rises by an amount of ~1.4 relative to its initial level [11]; considering the initial excited state fraction given for this experiment as 0.1–1 %, a value of 0.3% can be taken as an order-of-magnitude estimate for the electron-induced effect. With a vibrational cooling rate of ~1/0.5 s apparent from Fig. 19(a) of Ref [11], this indicates an excitation rate of ~1/170 s; using the applied electron density and electron beam overlap factor, a rate coefficient in the middle $10^{-8}$ cm$^3$ s$^{-1}$ range is obtained. Hence, the maximum rate coefficients for the two excitation curves shown in Fig. 9(b) are of similar order of magnitude.

The effect of residual-gas collisions on the internal excitation of the stored molecular ions is probed by the measurements shown in Fig. 10, where the electron beam is switched off after a long initial storage and cooling period of 22.5 s. The molecules are then left interacting with the residual gas alone for increasingly long periods of time and the resulting internal excitation is then probed through the size of the effective low-energy DR rate coefficient $\tilde{\alpha}_{\mathrm{DR}}(E_d^c,t)$ [Fig. 10(a)] and through CEI directly yielding the vibrational populations [Fig. 10(b)]. The DR rate coefficient $\tilde{\alpha}_{\mathrm{DR}}(E_d^c,t)$ is found to have much higher values than before the electron beam was switched off, while the vibrational populations remain close to their values after the initial cooling with $p_0$ ~0.75 (see Fig. 5 for $t$=22.5 s), showing only little vibrational heating. The observed small decrease of $p_0$ can be used to estimate the vibrational excitation cross section $\sigma_{\mathrm{ex}}^g$ in residual-gas collisions as

$$\sigma_{\mathrm{ex}}^g = -\ln[p_0(t)/p_0(t_{\mathrm{off}})]/(t-t_{\mathrm{off}})n_g v_i, \tag{17}$$

where $v_i$=1.42×10$^9$ cm/s ($E_i$=8.32 MeV) is the ion beam velocity and $n_g$=2.7×10$^6$ cm$^{-3}$ the residual gas density at the estimated pressure of 1×10$^{-10}$ mbar and 293 K. An upper limit of $\sigma_{\mathrm{ex}}^g$=1.7×10$^{-18}$ cm$^2$ can be derived from the measured populations using this relation.

These CEI results show that the changes in the vibrational populations through residual-gas collisions are ≲5% even over storage times of the order of 60 s, and thus much smaller than those caused by the collisions with low-energy electrons (Fig. 5). In the high-energy peak of the DR rate coefficient these small populations are expected to cause correspondingly small variations; on an absolute scale these can be neglected in comparison to other systematic errors, especially in the calibration procedure, since vibrational levels $v$=0, 1, and 2 are expected to have DR rate coefficients of similar magnitude in this range [8]. On the other hand, regarding the low-energy DR rate coefficient, the observed large change of $\tilde{\alpha}_{\mathrm{DR}}(E_d^c,t)$ in spite of the small relative population changes among the vibrational levels again underlines its high sensitivity on the internal vibrational excitation for $He_2^+$.

### F. Low-energy rate coefficients for superelastic collisions

As the effect of residual-gas collisions on the vibrational populations can be neglected against those from low-energy electron collisions, the CEI results of Fig. 5 can be modeled using the rate coefficients for electronic collisions only. We first consider only the effect of the vibrationally specific low-energy DR rate coefficients $\tilde{\alpha}_{\mathrm{DR}}^{(v)}$ at $E_d$=0. If we denote the number of stored ions in the state $v$ by $N_v$, the fraction of the ring circumference over which the stored ions interact with the electrons by $\eta=L/C$=0.027 (Sec. II), and the electron density at cooling by $n_e=n_e(E_d^c)$ (Table I), the relative populations are governed by the differential equation

$$\dot{N}_v = -\eta n_e \tilde{\alpha}_{\mathrm{DR}}^{(v)} N_v - k_X N_v, \tag{18}$$

where $k_X$ describes the loss processes except for DR, in particular DE-$R$ induced by the residual gas [Eq. (6)], assumed to be independent of $v$. Normalized populations obtained with this model are compared to the data in Fig. 5 for two cases, using for the DR rates the central values listed in Table II (broken curves) and values at the given error limits, using the lower limit for $v$=0 and the higher limits for $v$=1 and ≥2 (thin full curves); these latter values correspond to the strongest vibrational cooling effect compatible with the measured low-energy DR rates. Clearly, this model is compatible only with the decrease of the $v\geq 2$ population, but not with the time behavior observed for $v$=0 and 1. Hence, differential depletion by DR cannot be the only origin of the observed vibrational cooling.

In order to improve the agreement, we include in this model a crude description of SEC, considering only transitions with $\Delta v=-1$ and using the vibrationally independent value $\tilde{\alpha}_{\mathrm{SEC}}$ for the low-energy ($E_d$=0) SEC rate coefficient. This produces the modified equations

$$\dot{N}_0 = -\eta n_e \tilde{\alpha}_{\mathrm{DR}}^{(0)} N_0 - k_X N_0 + \eta n_e \tilde{\alpha}_{\mathrm{SEC}} N_1,$$

$$\dot{N}_1 = -\eta n_e (\tilde{\alpha}_{\mathrm{DR}}^{(1)} + \tilde{\alpha}_{\mathrm{SEC}}) N_1 - k_X N_1 + \eta n_e \tilde{\alpha}_{\mathrm{SEC}} N_2,$$

$$\dot{N}_2 = -\eta n_e (\tilde{\alpha}_{\mathrm{DR}}^{(2)} + \tilde{\alpha}_{\mathrm{SEC}}) N_2 - k_X N_2, \tag{19}$$

where the population in $v\geq 2$ is modeled by the single level $v$=2. Setting $\tilde{\alpha}_{\mathrm{SEC}}$=1.8×10$^{-7}$ cm$^3$ s$^{-1}$ in this model, we can reproduce the measured evolution also for the lower vibrational levels (full curves in Fig. 5), which shows that SEC with low-energy electrons essentially contributes to the observed vibrational relaxation.

The time dependence of the effective low-energy DR rate coefficient (Fig. 4) could be well reproduced using a similar model, although a systematic multicomponent fit was not feasible. With regard to the vibrationally specific DR rate coefficients $\tilde{\alpha}_{\mathrm{DR}}^{(v)}(0)$, the values within the error ranges of Table II yielding closest agreement were 4×10$^{-9}$ cm$^3$ s$^{-1}$ for $v$=0, 20×10$^{-9}$ cm$^3$ s$^{-1}$ for $v$=1, and 270×10$^{-9}$ cm$^3$ s$^{-1}$ for $v\geq 2$. Regarding the low-energy SEC rate coefficients $\tilde{\alpha}_{\mathrm{SEC}}^{(v)}(0)$ it improved the agreement to apply separate values of 1.8×10$^{-7}$ cm$^3$ s$^{-1}$ for $v$=1 and 5×10$^{-7}$ cm$^3$ s$^{-1}$ for $v\geq 2$. Separate $v$-dependent SEC rate coefficients are easily implemented in Eq. (19), and the higher value for SEC from $v\geq 2$ given above yields populations compatible with the data in Fig. 5. The inclusion of vibrational excitation in residual-gas collisions further improved the agreement, when excitations from $v$=0 into the levels $v'$=1 and $v'\geq 2$ were included with a branching ratio of 1:8;

an appropriate value of the cross section was found to be $\sigma_{ex}^{g}=2\times10^{-19}$ cm$^2$, in agreement with the upper-limit estimate in Sec. III E.

## IV. DISCUSSION

### A. Comparison to $^3$He $^4$He$^+$ results

In the previous TSR measurement on the isotopically asymmetric helium dimer ion $^3$He $^4$He$^+$, vibrational relaxation, mainly through radiative emission, could be achieved, leaving a residual excitation fraction for $v\geq3$ between 0.1% and 1% [11]. In the present experiment on $^4$He$_2^+$ the cooling through low-energy electron collisions yields a somewhat less complete vibrational relaxation, allowing us to give only a limit of $<5\%$ in $v\geq1$ for the residual excited fraction. Moreover, in contrast to $^3$He $^4$He$^+$, where also rotational radiative cooling occurred and clear signs of further rotational relaxation by low-energy electron collisions could be seen [11], the present experiment on $^4$He$_2^+$ does not allow us to identify specific effects of rotational relaxation, although it may proceed through electron collisions in parallel to the vibrational cooling. Altogether, we estimate that also the degree of rotational excitation remaining in the stored beam at long storage times will be somewhat higher than for $^3$He $^4$He$^+$.

The effective ($v$- and $J$-averaged) DR rate coefficient for $^4$He$_2^+$ at the strongest relaxation (Fig. 3, type-B data) shows an energy dependence and size very similar to the one for $^3$He $^4$He$^+$ [Fig. 10(a) of Ref. [11]]. In both cases almost the same structures are observed in the energy range of 1–40 eV. At very low energies, the statistical noise of the strongly relaxed $^4$He$_2^+$ measurement is considerably larger than for $^3$He $^4$He$^+$ and residual contributions from the weakly populated high-$v$ states with large DR cross sections must be considered in addition to the $v=0$ signal. Nevertheless, the clear structure for $^3$He $^4$He$^+$ at $\sim0.03$ eV does not seem to occur for $^4$He$_2^+$, whereas for the latter system indications of a resonance are observed near $10^{-3}$ eV. This points to different rovibrational resonance structures for the two species at low energies.

Regarding the high-energy structure in the DR rate peaking at $\sim7.5$ eV, Fig. 6(a), the $^4$He$_2^+$ data with strongest relaxation (type B) should be compared to those for $^3$He $^4$He$^+$. The peak seems to be shifted by $\sim0.5$ eV to higher energies for $^4$He$_2^+$; moreover, for $^3$He $^4$He$^+$ the peak is sharper and slightly more asymmetric than for $^4$He$_2^+$. It cannot be excluded that a similar, sharper structure could appear also for $^4$He$_2^+$ after even better internal relaxation of the stored ions. The peak rate coefficient for DR is found to be $\sim25\%$ smaller for $^4$He$_2^+$ as compared to $^3$He $^4$He$^+$. The observed DR structures at $\sim20$–35 eV, Fig. 6(b), are found to be very similar among both species, including the small narrow peak near 19 eV. An energy shift upward by $\sim0.5$ eV for $^4$He$_2^+$ is seen also here. The DE rate coefficients as a function of collision energy (Fig. 7) show very close agreement with each other, including the plateau value around 20 eV. The small intermediate plateau at $\sim6.5$ eV is not as clear for $^4$He$_2^+$ as for $^3$He $^4$He$^+$ [cf. Fig. 23(a) of Ref [11]], and the slopes of the signal as a function of energy are somewhat less steep for $^4$He$_2^+$; both may be signs of a slightly higher residual population in the excited vibrational levels for $^4$He$_2^+$.

The energy dependences of the rate for rovibrational excitation by electron collisions, Fig. 9(b), are found to be very similar between the two systems. In addition, estimates for the maximum of the excitation rate coefficients yield similar magnitudes of the order of a few $10^{-8}$ cm$^3$ s$^{-1}$ (Sec. III E).

### B. Comparison to previous storage ring results on $^4$He$_2^+$

As pointed out in Sec. III A, the most conspicuous difference between the present storage ring results on $^4$He$_2^+$ and the previous ones [10] on the same system observed at the ASTRID storage ring is the high degree of vibrational relaxation obtained here through low-energy electron collisions. Therefore, the energetic structures in the DR rate coefficient turn out to be similar to those in $^3$He $^4$He$^+$, which benefits from fast spontaneous radiative relaxation. In fact, the monotonic decrease of the DR rate as a function of the collision energy seen at ASTRID indicates the absence of any significant vibrational relaxation. This difference can be understood on the basis of the different experimental conditions encountered at TSR and ASTRID.

For this comparison, we note that in the present experiment the time scale for vibrational cooling by SEC, according to Sec. III F, is $\tau_{SEC}=(\eta n_e\tilde{\alpha}_{SEC})^{-1}\sim18$ s, while the time scale for excitation due to residual-gas collisions is given by $\tau_{ex}=(n_g v_i \sigma_{ex}^{g})^{-1}\geq153$ s. The cooling time scale $\tau_{SEC}$ is thus considerably shorter than $\tau_{ex}$, resulting in an overall cooling effect. At ASTRID, the beam lifetime (at $E_i=5.6$ MeV) was found to be about a factor of 5 shorter than the one in the present TSR experiment (see Sec. II); hence, the residual-gas density in the ASTRID experiment was about a factor of 5 higher, leading to stronger excitation with a time scale reaching down to $\sim30$ s. On the other hand, the cooling by low-energy electron collisions is expected to be slower by a factor of $\sim2$ because of the lower electron density at ASTRID ($n_e=8\times10^6$ cm$^{-3}$ [10]) and the higher electron temperature ($kT_\perp=22$ meV), assuming $\tilde{\alpha}_{SEC}$ to vary proportionally to $T_\perp^{-1/2}$. This shows that at ASTRID the time scale for vibrational cooling may well have been of similar size or even longer in comparison to that for heating by residual-gas collisions, so that the absence of any significant vibrational cooling for $^4$He$_2^+$ ions in that experiment can be rationalized. Moreover, at ASTRID a different type of ion source possibly producing more highly excited ions was used, and the $^4$He$_2^+$ ions were injected into the storage ring at a beam energy of only 150 keV and then accelerated there during 3.5 s [10], which may have increased their vibrational excitation at the beginning of electron cooling relative to that in the ion source.

In the previous TSR study on $^3$He $^4$He$^+$ [11], the high-energy peak of the DR rate coefficient was found to be higher by a factor of 2.8 than the one determined in the ASTRID measurement [10]. We have repeated the absolute calibration of the DR rate coefficient for this system using the same method as for $^4$He$_2^+$ described in Sec. II D.

This yielded $\alpha_{DR}^{abs}(E_d^{abs})=2.4(1)(5)\times10^{-8}$ cm$^3$ s$^{-1}$ at $E_d^{abs}=7.4$ eV, in good agreement with the previously determined result of $2.8(4)\times10^{-8}$ cm$^3$ s$^{-1}$ at 7.3 eV [11]. Moreover, we have carefully verified the validity of the assumptions underlying the calibration method in test experiments. This leads us to maintain our absolute values for the $He_2^+$ cross sections in spite of the disagreement with the ASTRID result found for this species.

### C. Comparison to theory

Predictions for the low-energy DR rate coefficient of the $He_2^+$ isotopologues are available from calculations [1] by multichannel quantum-defect theory (MQDT) covering the energy range of 0.0001 to 2 eV and dissociation via the three lowest neutral channels with $^3\Sigma_g^+$, $^1\Sigma_g^+$ and $^3\Pi_u$ symmetries (see Fig. 1). At a thermal energy equivalent to 300 K, the predicted cross section was $\sim1\times10^{-18}$ cm$^2$ which, multiplied by the thermal velocity of $\sim1\times10^7$ m/s, yields a thermal rate coefficient of $\sim1\times10^{-11}$ cm$^3$ s$^{-1}$. However, when a more detailed thermal average was performed over the computed rate coefficients, a higher value of $6.1\times10^{-11}$ cm$^3$ s$^{-1}$ was obtained. In addition, a rich structure from strong indirect DR peaks as well as the mentioned strong $v$ dependence were found, the $v=4$ cross section being about four orders of magnitude higher, corresponding to a thermal rate coefficient of the order of $10^{-7}$ cm$^3$ s$^{-1}$. The present result for the thermal, low-$v$ $^4He_2^+$ DR rate coefficient (Sec. III D) as well as the previous result [11] for $^3$He $^4$He$^+$, amounting to several $10^{-10}$ up to $10^{-9}$ cm$^3$ s$^{-1}$, appear to be significantly larger than predicted. Both for $^4He_2^+$ (Fig. 3) and for $^4He_2^+$ [11] no strong structures are experimentally observed, although, as pointed out above, the influence of residual population in higher $v$ levels with much higher DR rates leaves large uncertainties in this energy region. The derived high-$v$ ($\geq2$) thermal rate coefficient of $\sim10^{-7}$ cm$^3$ s$^{-1}$ can be considered to be in reasonable agreement with the theoretical prediction [1] for $v=4$.

Interestingly, the rate coefficients for vibrational deexcitation in low-energy electron collisions (SEC) on $^4He_2^+$ are found to be substantial even for $v=1$ (see Sec. III F), while the low-energy DR rate coefficients are found to be almost two orders of magnitude smaller (Sec. III D). Similarly, large rotational SEC rate coefficients were implied in Ref. [11] to explain the observed time dependence of $\tilde{\alpha}_{DR}(E_d^c)$ for $^3$He $^4$He$^+$. To our knowledge, no theoretical predictions of the low-energy SEC rate coefficients have been published for these ions. As the low DR rate coefficient is explained by the small Franck-Condon overlap with resonant, electronically doubly excited potentials, and SEC can often be understood through the autoionization following the capture into excited potentials leading also to DR, the high SEC rate coefficients may appear surprising. They can, however, be explained through strong electron capture rates into intermediate rovibrationally excited $He_2$ Rydberg states built on the ground state ionic core. These states would show only little (indirect [1]) DR because of weak predissociation through the doubly excited $He_2$ potentials, but could show strong autoionization into $He_2^+$ states with reduced vibrational (or rotational) quantum numbers.

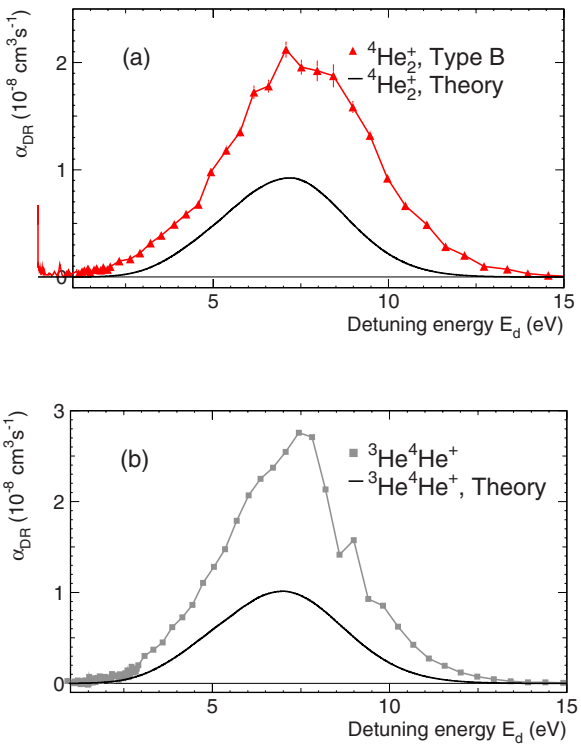


FIG. 11. (Color online) Rate coefficients for dissociative recombination $\alpha_{DR}$ from wave-packet calculations [8,9] for the vibrational ground state $v=0$ (smooth lines) in comparison to the corresponding experimental results for (a) $^4He_2^+$ (this work) and (b) $^3$He $^4$He$^+$ [11].

Recently, inelastic electron collision processes on $He_2^+$ at higher energy were calculated in the range of 1–15 eV, considering a large number of doubly excited neutral Rydberg potentials below the $A\ ^2\Sigma_g^+$ excited ionic potential. The wave-packet dynamics of the dissociation process in these doubly excited Rydberg potentials, including their autoionization, was analyzed yielding cross sections for DR [8] as well as for DE and vibrationally inelastic collisions [9] on a unified basis.

Compared to low-energy DR, the cross sections of these higher-energy processes vary much less as a function of the initial vibrational quantum number $v$ and differ from each other mainly by their energy dependence [8,9]. Therefore, the relaxation to greater than 95% $v=0$ population achieved in the present experiment can be expected to yield essentially the results for $v=0$. Moreover, the experimental electron energy spread is always small compared to the collision energy (full width at half maximum $\sim0.07$ eV at $E_d=1$ eV and $\sim0.2$ eV at $E_d=10$ eV, using the relation given in Sec. III A of Ref. [23]), and the energetic structures in the calculated cross sections are wide compared to this energy resolution. Hence, we simply multiply these cross sections with the collision velocity to obtain the predicted rate coefficients.

For the DR rate coefficient of $^4He_2^+$, the theoretical result [8] yields a peak extending over $\sim2.5-11.5$ eV with a maximum of $0.91\times10^{-8}$ cm$^3$ s$^{-1}$ at 7.1 eV [Fig. 11(a)]. This peak is situated $\sim0.5$ eV below the experimental one and predicts a rate coefficient smaller than the measured maximum by a factor of 2.1. The main deviation from the experi-

ment appears at the higher energies, where the experimental peak also extends further up by ~1.5 eV. The calculated DR rate coefficient for $^3$He $^4$He$^+$ [8] is found to be higher by ~10% at a maximum shifted down in energy by ~0.2 eV [Fig. 11(b)]. The calculation does not reproduce the sharper peak structure found experimentally for the asymmetric isotopologue and the calculated rate coefficient at the peak is smaller than the experimental value by a factor of 2.6. Although this calculation agrees much better with the other available storage ring measurement for $^3$He $^4$He$^+$ [10], we are led to maintain our absolute calibration as discussed in Sec. IV B. Thus, we find a significant discrepancy in the detailed comparison with the recent wave-packet calculations regarding the DR for both isotopologues.

The conventional DE process of $He_2^+$, consisting of direct electron impact excitation to the $A\ ^2\Sigma_g^+$ ionic potential and the subsequent dissociation of the excited ion, is expected to have an energetic onset at ~6 eV for $v=0$ because of the required Franck-Condon overlap and to reach a plateau near 10 eV [9]. The experimental DE rate coefficient (Fig. 7) rises already at ~3 eV, much below the energy corresponding to the direct DE process, and shows an intermediate small shoulder at ~6 eV. The contributions below 6 eV can be explained by resonance-enhanced DE following electron capture into the same doubly excited neutral Rydberg potentials leading to DR, followed, however, by autoionization in a later stage of the dissociation process. This is clearly supported by the wave-packet calculations [9], which yield peaks due to resonance-enhanced DE extending over the range ~3.5–10.5 eV (Fig. 12). In a detailed comparison, the calculated structure of resonance-enhanced DE [9] rises at somewhat higher energies than the experimental DE rate. The rate coefficients at the peaks of these structures are close to those observed in the vicinity of the intermediate shoulders. Thus, a general agreement regarding the size of the resonance-enhanced DE process is found with the recent wave-packet calculations, while the energetic dependence at the low-energy limit of the process appears to be somewhat different from the predictions. At higher energies ($E_d$ >10 eV), the DE process is nonresonant and therefore not described by the theoretical model. It is worthwhile noting that in the present experiment the DR and DE rate coefficients are obtained using a single absolute calibration procedure for both, the uncertainty of the *relative* rates being essentially given by the statistical uncertainty of only ~5%. Hence, the observed discrepancy regarding high-energy DR (Fig. 11), together with the reasonable agreement between the theoretical and experimental DE rate coefficients up to ~6 eV (Fig. 12), could indicate a theoretical underestimation of the ratio between DR and resonant DE. Considering the good agreement with theory regarding resonant DE in the present measurement, we would then be additionally supported in our suggestion that the apparent agreement regarding high-energy DR between theory [8] and the experimental result of Ref. [10] is fortuitous.

The wave-packet calculations [9] also predict a peak in the cross section for vibrational excitation by electron collisions in the range ~2–8 eV with a maximum at ~4.5 eV (Fig. 13). This reproduces well the shape of the excitation functions of Fig. 9(b). The predicted maxima of the rate coefficients of $\sim 4\times10^{-8}$ cm$^3$ s$^{-1}$ lie in the range estimated for the peaks observed on $^4He_2^+$ and $^3$He $^4$He$^+$ in Sec. III E.

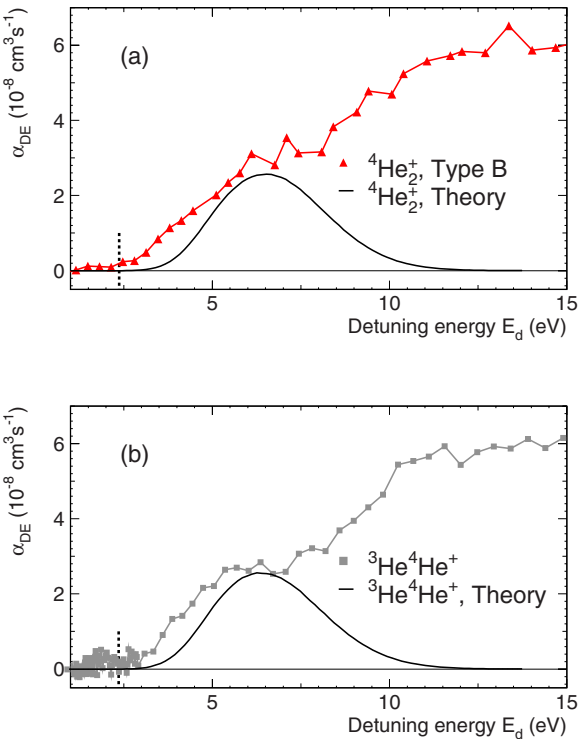


FIG. 12. (Color online) Rate coefficients for dissociative excitation $\alpha_{DE}$ from wave-packet calculations [9] for the vibrational ground state $v=0$ (smooth lines) in comparison to the corresponding experimental results for (a) $^4He_2^+$ (this work) and (b) $^3$He $^4$He$^+$ [11] (cf. Sec. III C). The vertical lines mark the ground state dissociation thresholds.

## V. CONCLUSIONS

For the study of electron collision processes on diatomic molecular ions, the helium dimer ion presents an interesting case at the transition between the simplest case of a one-electron molecular core (the hydrogen molecular ion) and heavier diatomics with a complex many-electron structure. Together with a previous experiment [11], energy-resolved data are now available for the principal types of inelastic electron collisions on this ion at low and intermediate energy, ranging up to ~40 eV, for both symmetric and asymmetric isotopologues and with populations of excited initial vibrational states reduced to a few percent or less.

In the low-energy region, the theoretically predicted large vibrational dependence of the DR rate coefficients for $He_2^+$ is confirmed. The possibility of verifying the DR calculations in this energy range is limited by the relatively large influence of the remaining, even small, high-$v$ populations. The measured DR rate coefficients appear to be slightly larger and to feature less structure from indirect DR than predicted. On the other hand, substantial rates, even for the lowest $v$ levels, are found for vibrational and rotational SEC, which present the basis of the strong electron-induced internal molecular relaxation observed, greatly benefiting the experimental method.

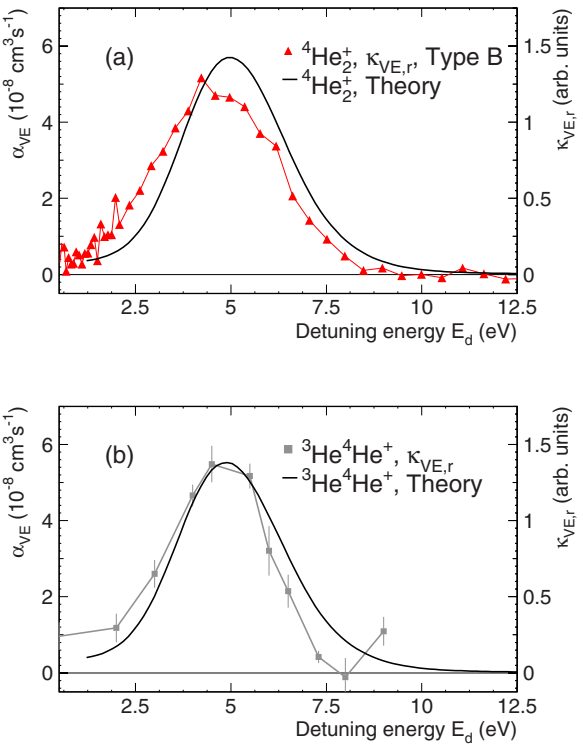


FIG. 13. (Color online) Rate coefficients for vibrational excitation $\alpha_{VE}$ from wave-packet calculations [9] for the vibrational ground state $v=0$ (smooth lines) in comparison to the corresponding, arbitrarily scaled, experimental results for (a) $^4He_2^+$ (this work) and (b) $^3He\ ^4He^+$ [11] (cf. Sec. III E).

At higher energies, the doubly excited neutral potentials attached to the lowest excited state of $He_2^+$ govern the collisions over a wide range up to ~18 eV. Of the three competing processes, DR shows a clear isotope effect with the peak rate coefficient found to be reduced by ~25% for $^4He_2^+$ with respect to $^3He\ ^4He^+$. Smaller isotopic differences are found in the DE rate coefficient and in the energetic dependence of the vibrational excitation. The recent series of time-dependent calculations [8,9] regarding these inelastic collisions offers a unique opportunity to verify the concepts of fast electronic and nuclear dynamics applied to model these processes. The basic observed dependences are well reproduced by these calculations; however, larger discrepancies still occur for the cross section and the isotope effects in DR and for the energetic onset of DE following resonant electron capture. These discrepancies could motivate extensions of the theoretical model, such as including the influence of nonadiabatic interactions mixing the autoionization probabilities between the several relevant neutral doubly excited states.

Regarding the ensemble of the three competing electronic collision processes in this energy range, the comparison of experimental results and predictions made possible now for the helium dimer ion appears to be the most complete one available in the literature. For the hydrogen molecular ion $HD^+$, which has a simpler core structure, the experimental high-energy DR structure [25] was compared to MQDT calculations [26], and good agreement was found. However, similarly detailed comparisons on DE and vibrational excitation, as well as calculations using the wave-packet approach at higher collision energy than so far considered in this case [27], are not available. To extend this comparison to $HD^+$ appears of great interest in order to further improve the understanding of the fast quantum dynamics in highly excited small molecules.

The range above ~18 eV, where the higher excited $He_2^+$ potentials become important and new structure arises as shown in Fig. 6(b), has so far been studied only experimentally. Calculations on the collision cross sections in this energy range are not available, but appear promising considering the variety of additional dynamic phenomena possible through the numerous interacting ionic potentials [12,28] (see Fig. 2 of Ref. [11]).

Future experimental work on helium dimer ions using fragment-imaging techniques appears of interest, in particular regarding the final state branching ratios. At low energies, this could also shed light on the role of rotations for $^4He_2^+$, which remains largely unexplored in the present storage ring experiment, while rotational cooling by electron collisions was clearly found in the previous measurements with a stored $^3He\ ^4He^+$ beam.

## ACKNOWLEDGMENTS

The authors thank Ann E. Orel, Ioan F. Schneider, and Jeanna Royal for useful discussions and theoretical data. This work has been funded in part by the German Israel Foundation for Scientific Research (GIF) under Contract No. I-707-55.7/2001. H.B.P. acknowledges support from the European Community program IHP under Contract No. HPMF-CT-2002-01833, and D.Sch. acknowledges support by the Weizmann Institute through the Joseph Meyerhoff program. X.U. received support from the FRS-FNRS.

[1] L. Carata, A. E. Orel, and A. Suzor-Weiner, Phys. Rev. A **59**, 2804 (1999).
[2] P. C. Stancil, S. Lepp, and A. Dalgarno, Astrophys. J. **509**, 1 (1998).
[3] R. Deloche, P. Monchicourt, M. Cheret, and F. Lambert, Phys. Rev. A **13**, 1140 (1976).
[4] S. Krohn, Z. Amitay, A. Baer, D. Zajfman, M. Lange, L. Knoll, J. Levin, D. Schwalm, R. Wester, and A. Wolf, Phys. Rev. A **62**, 032713 (2000).
[5] J. Xie, B. Poirier, and G. I. Gellene, J. Chem. Phys. **122**, 184310 (2005).
[6] J. S. Cohen, Phys. Rev. A **13**, 86 (1976).
[7] R. S. Mulliken, Phys. Rev. **136**, A962 (1964).
[8] J. Royal and A. E. Orel, Phys. Rev. A **72**, 022719 (2005).
[9] J. Royal and A. E. Orel, Phys. Rev. A **75**, 052706 (2007).
[10] X. Urbain, N. Djuric, C. P. Safvan, M. J. Jensen, H. B. Peder-

sen, L. V. Sogaard, and L. H. Andersen, J. Phys. B **38**, 43 (2005).
[11] H. B. Pedersen *et al.*, Phys. Rev. A **72**, 012712 (2005).
[12] J. Ackermann and H. Hogreve, Chem. Phys. **157**, 75 (1991).
[13] D. Habs *et al.*, Nucl. Instrum. Methods Phys. Res. B **43**, 390 (1989).
[14] T. S. Green, Rep. Prog. Phys. **37**, 1257 (1974).
[15] M. Grieser *et al.*, Nucl. Instrum. Methods Phys. Res. A **328**, 160 (1993).
[16] S. Pastuszka *et al.*, Nucl. Instrum. Methods Phys. Res. A **369**, 11 (1996).
[17] A. Wolf, S. Krohn, H. Kreckel, L. Lammich, M. Lange, D. Strasser, M. Grieser, D. Schwalm, and D. Zajfman, Nucl. Instrum. Methods Phys. Res. A **532**, 69 (2004).
[18] F. Sprenger, M. Lestinsky, D. A. Orlov, D. Schwalm, and A. Wolf, Nucl. Instrum. Methods Phys. Res. A **532**, 298 (2004).
[19] R. Wester, F. Albrecht, M. Grieser, L. Knoll, R. Repnow, A. Wolf, A. Baer, J. Levin, Z. Vager, and D. Zajfman, Nucl. Instrum. Methods Phys. Res. A **413**, 379 (1998).
[20] L. Lammich *et al.*, Phys. Rev. A **69**, 062904 (2004).
[21] W. Cencek and J. Rychlewski, J. Chem. Phys. **102**, 2533 (1995).
[22] Z. Amitay *et al.*, Phys. Rev. A **60**, 3769 (1999).
[23] G. Kilgus, D. Habs, D. Schwalm, A. Wolf, N. R. Badnell, and A. Müller, Phys. Rev. A **46**, 5730 (1992).
[24] A. Lampert, A. Wolf, D. Habs, J. Kenntner, G. Kilgus, D. Schwalm, M. S. Pindzola, and N. R. Badnell, Phys. Rev. A **53**, 1413 (1996).
[25] A. Al-Khalili *et al.*, Phys. Rev. A **68**, 042702 (2003).
[26] I. F. Schneider, C. Strömholm, L. Carata, X. Urbain, M. Larsson, and A. Suzor-Weiner, J. Phys. B **30**, 2687 (1997).
[27] A. E. Orel, Phys. Rev. A **62**, 020701(R) (2000).
[28] A. D. O. Bawagan and E. R. Davidson, Chem. Phys. Lett. **266**, 499 (1997).